Light emission and enhanced nonlinearity in nanophotonic waveguide circuits by III–V/silicon-on-insulator heterogeneous integration

G. Roelkens,[1,a)] L. Liu,[1] D. Van Thourhout,[1] R. Baets,[1] R. Nötzel,[2] F. Raineri,[3] I. Sagnes,[3] G. Beaudoin,[3] and R. Raj[3]
[1]*Photonics Research Group (INTEC), Ghent University-IMEC, Sint-Pietersnieuwstraat 41, Ghent B-9000, Belgium*
[2]*OED Group, Technical University Eindhoven, Den Dolech 2, Eindhoven 5600 MB, The Netherlands*
[3]*Laboratoire de Photonique et de Nanostructures, CNRS UPR20, Route de Nozay, Marcoussis 91460, France*

(Received 29 April 2008; accepted 11 June 2008; published online 15 August 2008)

The heterogeneous integration of a III–V thin film on top of a silicon-on-insulator (SOI) optical waveguide circuit by means of adhesive divinylsiloxane-benzocyclobutene (DVS-BCB) die-to-wafer bonding is demonstrated, thereby achieving light emission and enhanced nonlinearity in ultracompact SOI cavities. This approach requires ultrathin DVS-BCB bonding layers to allow the highly confined optical mode to overlap with the bonded III–V film. The transfer of sub-100-nm III–V layers using a 65 nm DVS-BCB bonding layer onto SOI racetrack resonator structures is demonstrated. Spontaneous emission coupled to a SOI bus waveguide, spectrally centered around the resonator resonances, is observed by optically pumping the III–V layer. Strong carrier-induced nonlinearities are observed in the transmission characteristics of the III–V/SOI resonator structure. The all-optical control of an optical signal in these III–V/SOI resonators is demonstrated. © *2008 American Institute of Physics*. [DOI: 10.1063/1.2967832]

I. INTRODUCTION

Silicon on insulator (SOI) is emerging as a disruptive technology for the realization of photonic integrated circuits comprising both passive and active functionalities. This is driven by the fact that standard complementary metal-oxide semiconductor (CMOS) technology can be used to fabricate photonic integrated circuits, thereby improving the yield, reproducibility, and cost of the fabrication.[1] While passive optical functions such as wavelength filters[2,3] and active optical functions such as light modulation[4] can be realized in silicon, light detection, amplification, and emission require other materials to be integrated on the SOI waveguide platform, i.e., III–V (Ref. 5) or germanium[6] for light detection and III–V material for light emission and amplification.[7,8] The high refractive index contrast between the silicon waveguide core ($n=3.45$ at 1.55 μm) and the SiO_2 cladding layer ($n=1.45$ at 1.55 μm) is ultimately exploited by using nanophotonic strip waveguides, which are defined by completely etching through a $\lambda/2n$ thick silicon waveguide layer.[1] This results in a single mode waveguide with cross-sectional dimensions on the order of 500×200 nm^2 (for operation at the 1.55 μm telecommunication wavelength) with a very high omnidirectional refractive index contrast, which allows making wavelength-scale optical functions. This miniaturization further leverages the cost of the photonic integrated circuit as more photonic integrated circuits can be obtained from a single SOI wafer. The integration of light emitters on the SOI waveguide platform can be achieved in different ways. In Ref. 7 we demonstrated for the first time the heterogeneous integration of an InP/InGaAsP Fabry–Pérot-type laser diode on and coupled to a nanophotonic SOI waveguide circuit using a divinylsiloxane-benzocyclobutene (DVS-BCB) adhesive bonding. We also demonstrated the integration of a III–V microdisk laser onto a SOI nanophotonic waveguide circuit.[9] Recently, the work of Intel/UCSB has received a lot of attention, in which a III–V epitaxial layer is transferred onto a SOI rib waveguide structure.[8,10] While integrated optoelectronic devices were realized this way, the use of SOI rib waveguide structures limits the further downscaling of the size of the photonic integrated circuit due to the limited refractive index contrast that can be realized in this single mode rib waveguide structure. In this paper we present for the first time the realization of light emission from ultracompact III–V/SOI cavities based on the nanophotonic strip waveguide platform, resulting in devices with a typical footprint of 100 μm^2. In Ref. 9 devices of about the same size were realized in a bonded III–V film. The main difference between both approaches is that in this case the cavity is defined in the SOI waveguide layer instead of in the III–V waveguide layer, which makes the III–V postprocessing very straightforward and possibly CMOS compatible. By locating the cavity in the SOI waveguide layer, one can also benefit from the high-resolution deep UV lithography to define the cavity. Besides light emission around 1.55 μm from a SOI cavity with an InP/InGaAsP layer structure bonded on top, a strong nonlinear effect in the transmission spectrum of the III–V/SOI resonators is observed due to the creation of carriers in the bonded III–V layer. As this is due to a linear photon absorption process, the required optical power to observe nonlinear behavior is lower than what is typically used in all-silicon nonlinear components, which rely on the weak two-photon absorption or the Kerr effect in silicon. This enhanced nonlinearity will be further demonstrated by showing that the transmission spectrum of a III–V/SOI resonator can be modified drastically in an all-optical way, leading to effi-

[a)]Electronic mail: gunther.roelkens@intec.ugent.be.

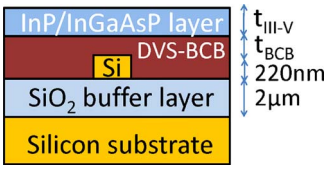

FIG. 1. (Color online) Cross section of the considered III–V/SOI nanophotonic waveguide structure.

cient all-optical modulation of light. The paper is organized as follows. In Sec. II the properties of the waveguide structure used in this paper will be outlined, while in Sec. III the bonding technology that is used for the integration of the III–V layer on top of the SOI nanophotonic waveguide circuit will be discussed. In Sec. IV the results on light emission from the III–V/SOI cavities will be presented, while in Sec. V the nonlinear transmission properties of the cavity will be demonstrated. In Sec. VI the all-optical control of optical signals in III–V/SOI cavities will be described.

II. III–V/SOI NANOPHOTONIC WAVEGUIDE STRUCTURES

The considered III–V/SOI nanophotonic waveguide structure is schematically depicted in Fig. 1. The SOI nanophotonic strip waveguide structure used consists of a 220 nm thick silicon waveguide layer on top of a 2 μm thick SiO_2 buffer layer to prevent the leakage of light to the silicon substrate. In order to achieve a single mode operation, 500 nm wide strip waveguides are used. The integration of a high refractive index III–V layer on top of the SOI nanophotonic waveguide can drastically change the modal properties of the waveguide structure. Indeed, the III–V bonded film ($n_{\text{III–V}} \approx 3.3$) behaves as a quasisubstrate into which the SOI guided mode (with an effective index of about 2.5 for the quasitransverse electric guided mode) can leak. Only by making the III–V film sufficiently thin can a substantial leakage of light into the bonded III–V film be avoided. The leakage loss of the III–V/SOI mode into the bonded III–V film plays an important role especially in the racetrack resonator cavity design presented in this paper as it can dramatically lower the quality factor of the racetrack resonator resonances. In Fig. 2(a), the radiation loss of the quasitransverse electric mode propagating in a bent III–V/SOI waveguide structure is plotted as a function of bend radius and III–V overlay thickness. These simulations were performed using a home-built full vectorial mode solver based on a finite element method, with perfectly matched layer absorbing boundary conditions. The DVS-BCB spacing ($n_{\text{DVS-BCB}}=1.54$) between the III–V overlay and silicon waveguide core is fixed to 50 nm. It is clear that in order to reduce the leakage loss, the bonding layer thickness can be increased. However, this deteriorates the overlap of the guided mode with the III–V layer, as shown in Fig. 2(b).

From these simulations one can conclude that in order to get a high confinement factor (>10%) in the bonded III–V film (such a high value has to be assumed, as only the overlap with InGaAsP active layers contributes to light emission and nonlinear operation, which only accounts for a small fraction—typically 30%—of the total InP/InGaAsP layer

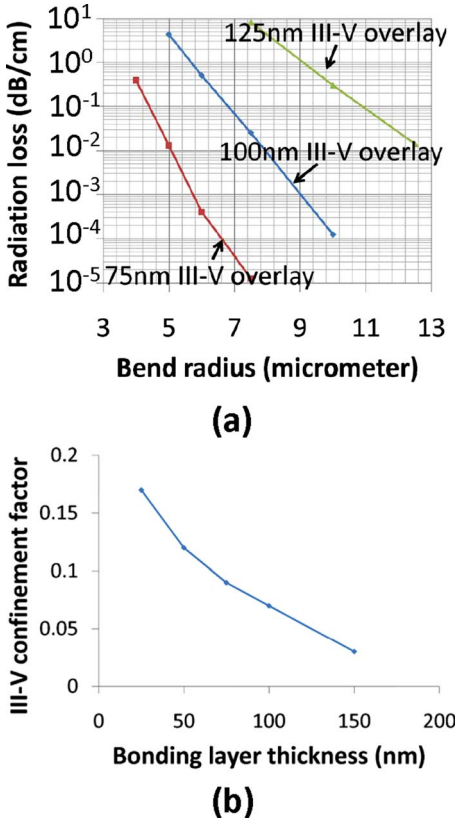

FIG. 2. (Color online) (a) Simulation of the radiation loss of the quasi-TE guided mode in a bent waveguide structure as a function of bend radius and III–V overlay thickness ($t_{\text{BCB}}=50$ nm) and (b) the influence of the DVS-BCB bonding layer thickness on the quasi-TE guided mode confinement factor in the III–V layer (bend radius of 5 μm, $t_{\text{III–V}}=75$ nm).

stack thickness, as will be shown later) while keeping the radiation losses low for a 5 μm bent waveguide in order not to reduce the quality factor of the resonator, the bonded III–V film has to be sub-100-nm thick and the bonding layer thickness has to be in the order of 50 nm. The E_x component of the quasitransverse electric (quasi-TE) mode profile and the E_y-component of the quasitransverse magnetic (quasi-TM) mode profile of a III–V/SOI bent waveguide (radius of 5 μm, waveguide width of 500 nm, an InP/InGaAsP overlay of 80 nm, and a bonding layer thickness of 65 nm) are plotted in Figs. 3(a) and 3(b), respectively. This waveguide cross section reflects the structure of the fabricated devices, as will be outlined in the following section. The mode profile of the quasi-TE and quasi-TM modes differs substantially in this high refractive index contrast waveguide structure. As the quasi-TM mode is less confined to the high index waveguide core, it is more affected by the waveguide surface roughness and radiation bending loss than the quasi-TE mode. Therefore, in Secs. IV–VI the focus will be on TE polarized light.

III. DVS-BCB BONDING TECHNOLOGY

The heterogeneous integration of a III–V film on top of a SOI waveguide substrate was realized using an epitaxial layer transfer technique based on DVS-BCB die-to-wafer bonding.[11] As an ultrathin bonding layer thickness is required, the most critical step in the process is the removal of particles pinned on the SOI waveguide circuit and the InP/

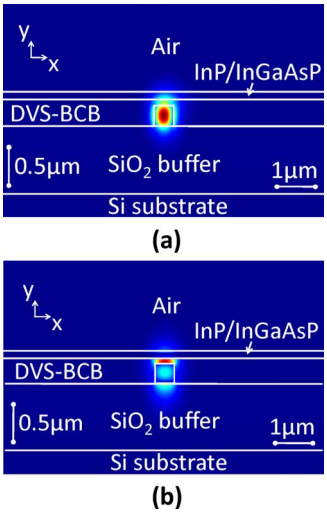

FIG. 3. (Color online) (a) The E_x-component of the quasi-TE mode profile and (b) the E_y-component of the quasi-TM mode profile of a III–V/SOI bent waveguide with a bend radius of 5 μm, waveguide width of 500 nm, InP/InGaAsP overlay $t_{\mathrm{III-V}}$ of 80 nm, and bonding layer thickness t_{BCB} of 65 nm.

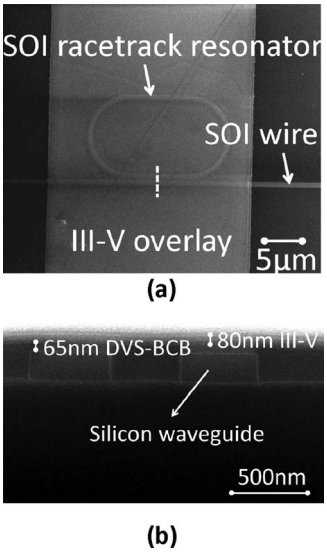

FIG. 4. (a) Scanning electron microscope top view image of a heterogeneous III–V/SOI microcavity and (b) a cross section of the layer structure at the dashed line in the top view image.

InGaAsP epitaxial layer stack, which would otherwise result in large unbonded areas. Particles on the SOI waveguide circuit were removed by immersing the SOI waveguide circuit into a standard clean-1 solution (SC-1, $1NH_3:4H_2O_2:20H_2O$ at 70 °C) for 15 min. This lifts off particles from the SOI surface and renders the surface hydrophilic. On the III–V surface, a sacrificial InP/InGaAs layer pair grown on top of the InP/InGaAsP active layer structure is removed by wet etching using HCl and $1H_2SO_4:1H_2O_2:18H_2O$, respectively. This leaves a particle- and contamination-free surface for bonding. After particle removal and surface conditioning, a solution of cyclotene 3022–25 DVS-BCB and mesitylene in a 2:3 ratio is spin coated on top of the SOI waveguide circuit. Diluting cyclotene 3022–35 DVS-BCB in mesitylene allows achieving the ultrathin bonding layers required in this application.[11] After a prebake at 150 °C to evaporate the remaining solvents in the spin coated layer, the III–V die is attached to the SOI waveguide circuit (epitaxial layers oriented downward) and the III–V/SOI stack is cured at 250 °C in a nitrogen environment for 1 h. After curing the DVS-BCB film, the InP growth substrate of the III–V die is removed by a combination of mechanical grinding and wet etching using $3HCl:H_2O$ until an InGaAs etch stop layer is reached. After the removal of the InGaAs etch stop layer using $1H_2SO_4:1H_2O_2:18H_2O$, the thin InP/InGaAsP active layer is left bonded on top of the SOI waveguide circuit. Lithographic definition of the areas where the bonded film should be removed in combination with wet etching leaves the III–V film only on top of the SOI waveguide circuit. The transfer of thin film III–V layers was successfully demonstrated using this process. An experimental realization of a sub-100-nm III–V bonded film using a 65 nm DVS-BCB bonding layer on top of a SOI racetrack resonator waveguide circuit is shown in Fig. 4.

IV. LIGHT EMISSION FROM AN ULTRACOMPACT III–V/SOI CAVITY

In this section the light emission properties of an ultracompact III–V/SOI racetrack resonator structure are outlined. The III–V film bonded on top of the SOI racetrack resonator circuit consists of a 20 nm active InGaAsP layer with a band gap wavelength of 1.55 μm, surrounded by two InP cladding layers of 30 nm. This active layer structure was bonded onto a SOI racetrack resonator cavity, as shown in Fig. 4. The radius of the bends in the racetrack cavity is 5 μm, while the directional coupler section length was varied. The confinement factor of the optical mode in the InGaAsP active layer is calculated to be 3%. In order to assess the light emission properties of the III–V/SOI ultracompact cavity, the III–V film was optically pumped from the surface of the optical circuit using a 660 nm fiber coupled red laser source. The light emission coupled to the SOI bus waveguide is collected from the waveguide facet using a lensed fiber. The spectrum of the spontaneous emission from a III–V/SOI racetrack resonator with a directional coupler section length of 4 μm is shown in Fig. 5(a), showing clearly that the spontaneous emission is spectrally located around the cavity resonances. Both quasi-TE and quasi-TM resonances are observed, as indicated in the spectrum. However, the quality factor of the quasi-TM polarized resonances is much lower and decreases with increasing wavelength (no more resonances can be observed for wavelengths longer than 1560 nm). This is related to the large difference in mode profile between the quasi-TE and quasi-TM modes, as discussed in Sec. II. In Fig. 5(b), the optical output power coupled to the SOI bus waveguide is plotted as a function of the estimated pump power that is absorbed in the III–V film for a racetrack resonator with a directional coupler section of 1 μm versus 4 μm. A 15 μm diameter pump spot is used. As only the carriers generated above the racetrack resonator waveguide contribute to the light emission in the SOI bus waveguide, in principle, much lower pump powers can be obtained by using a donut-shaped pump beam. A theoretical 9 dB coupling efficiency between the lensed fiber and the 3 μm wide SOI bus waveguide was assumed to derive a lower boundary for the optical power propagating in the SOI bus waveguide

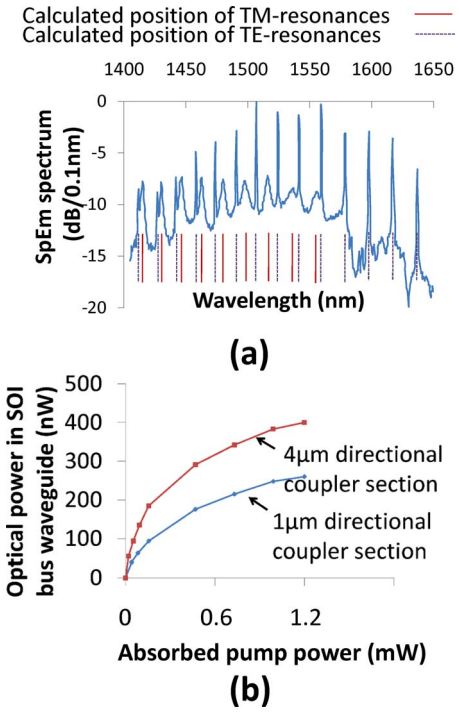

FIG. 5. (Color online) (a) Spectrum of the spontaneous emission coupled to the SOI bus waveguide and (b) optical power coupled to the SOI bus waveguide (single sided) as a function of the pumping power for two different resonator designs.

(single sided). From this measurement it is clear that the optical output power scales with the directional coupler length as the coupling coefficient to the SOI bus waveguide is higher for the 4 μm directional coupler section (together with the larger active volume of the cavity). No lasing was obtained in these devices due to the inefficient optical pumping of the resonator. This would require an in-plane pumping approach, using the silicon waveguide layer to pump the resonator structure (e.g., using a 1300 nm pump laser source). Efficient in-plane optical pumping can only be achieved by modifying the resonator layout to achieve a large extinction ratio for the pump laser (near critical coupling) while having a high quality factor resonance in the 1550 nm wavelength range. This lies, however, outside the scope of this paper.

V. NONLINEAR TRANSMISSION OF A III–V/SOI RACETRACK RESONATOR CAVITY

Besides for use as an ultracompact light emitter, III–V/SOI cavities show strong nonlinear behavior. This is due to the absorption that takes place in the III–V active layers when injecting light with a wavelength shorter than the band gap wavelength of the III–V active layers. This absorption process creates free carriers in the III–V active layer, which reduce the refractive index of the III–V active layer material due to the plasma dispersion effect, band filling, and band gap shrinkage. The reduction in the guided mode effective index results in a blueshift in the resonance spectrum, and hence results in a change in transmission as a function of the density of the free carriers or as a function of the injected optical power. Indeed, the transmission characteristic $T(\lambda)$ of the III–V/SOI cavity can be written as

$$T(\lambda) = \left| \sqrt{1-\kappa^2} - \frac{\kappa^2 \exp\left(-\frac{\alpha_c L_c}{2}\right)\exp(-j\varphi)}{1-\sqrt{1-\kappa^2}\exp\left(-\frac{\alpha_c L_c}{2}\right)\exp(-j\varphi)} \right|^2 . \quad (1)$$

With $\varphi=(2\pi/\lambda)\mathrm{Re}(n_{\mathrm{eff}})L_c$, λ is the wavelength, n_{eff} is the complex effective index of the quasi-TE mode, and L_c is the circumference of the resonator cavity. In Eq. (1), κ^2 represents the power coupling at the directional coupler section and $\alpha_c=(4\pi/\lambda)\mathrm{Im}(n_{\mathrm{eff}})$ is the power loss per length unit in the racetrack resonator cavity. As the creation of free carriers both in the III–V overlay (due to a linear absorption process) and in the silicon waveguide core (due to two-photon absorption) decreases the material refractive index (and hence the effective index), the resonances occurring at $\varphi=2m\pi$ appear at shorter wavelengths for larger carrier densities. In this analysis the heating of the waveguide structure due to the thermal relaxation of the generated free carriers and the nonradiative recombination was not included. The heating of the waveguide structure increases the effective index due to the thermo-optic effect, thereby inducing again a redshift in the resonances. While the carrier induced blueshift is dominant at low optical input powers (until about 500 μW waveguide coupled power, as will be demonstrated below), the thermo-optic effect takes over at high optical input powers due to the two-photon absorption in the silicon waveguide. Besides a spectral blueshift due to the reduction in the real part of the guided mode effective index, the absorption of the III–V active layer is bleached, which results in resonances with a higher quality factor when the input power is increased. These effects are demonstrated in this section. The III–V layer structure used in this experiment consists of three 10 nm thick InGaAs quantum wells with a band gap wavelength of 1.55 μm separated by 10 nm barrier layers and 7 nm InP cladding layers. This layer structure was transferred on top of a SOI racetrack resonator by means of the process outlined in Sec. III. The confinement factor of the guided mode in the InGaAsP quantum wells was calculated to be 5.2%. A high resolution fiber-to-fiber transmission spectrum of a III–V/SOI racetrack resonator structure with a 3 μm long directional coupler section is shown in Fig. 6 for 6 and −7 dBm fiber coupled powers. Light was coupled from the optical fiber to the SOI waveguide circuit using a one-dimensional diffractive grating structure,[12] which selectively couples quasi-TE polarized light into the waveguide circuit. An identical grating structure was used for coupling out the light exiting the through port of the racetrack resonator structure. The transmission spectrum of the double diffractive grating coupler structure (without intermediate resonator) is shown as an overlay. As can be clearly seen from the −7 dBm fiber

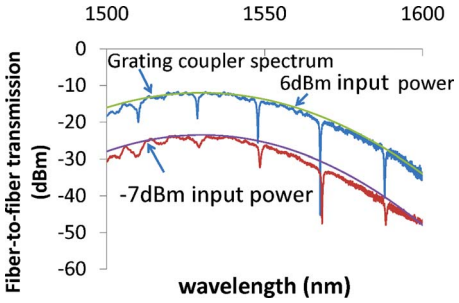

FIG. 6. (Color online) Fiber-to-fiber transmission spectrum of a III–V/SOI racetrack resonator.

coupled power curve, the extinction ratio and the quality factor of the resonances change significantly with the resonance wavelength. This is due to absorption in the InGaAsP quantum wells with a band gap wavelength of 1.55 μm and the decreasing power coupling at the directional coupler for shorter wavelengths. While the resonance around 1568 nm has an extinction ratio larger than 10 dB, the absorption and reduced optical coupling at shorter wavelengths cause the racetrack resonator to become undercoupled, thereby reducing the extinction ratio. At wavelengths shorter than 1510 nm, no more resonance dips can be observed. Increasing the optical input power tends to bleach this absorption, thereby creating distinct resonances, also at shorter wavelengths. This enhancement in the quality factor of the resonances for higher optical input powers can be clearly observed in the 6 dBm optical input power curve. Also the blueshift in the resonances for higher optical input powers can be observed. A close-up of the racetrack resonator transmission around the resonances at wavelengths of 1548 and 1568 nm, separated by one free spectral range and spectrally lying on the Urbach tail of the III–V quantum wells, is shown in Figs. 7(a) and 7(b), respectively, for various power levels in the SOI input waveguide. The increase in extinction ratio for increasing optical power, together with the blueshift in the resonance

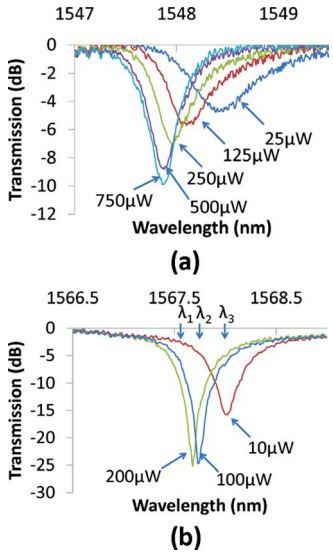

FIG. 7. (Color online) Transmission characteristic of the III–V/SOI racetrack resonator as a function of optical input power in the SOI waveguide for the resonances around (a) 1548 nm and (b) 1568 nm. Strong carrier induced nonlinearity can be observed.

spectrum, can be observed for low input powers in the SOI waveguide. Further increasing the optical input power tends to shift the resonance spectrum back to longer wavelengths due to the thermo-optic effect. The maximum carrier induced blueshift that could be achieved is about 0.6 nm around the 1548 nm resonance and 0.3 nm around the 1568 nm resonance. As a comparison, DVS-BCB coated SOI racetrack resonators without a III–V overlay only show a redshift in the transmission spectrum for increasing optical input powers, as in continuous wave operation, the two-photon absorption induced thermo-optic effect dominates the plasma dispersion effect based carrier blueshift in the silicon waveguide.[13]

The carrier induced blueshift and absorption bleaching result in strong nonlinear transmission characteristics, as shown in Fig. 7, where for various transmission curves the wavelength was varied and the optical input power was fixed. Applications for this nonlinear behavior can, however, be identified better by fixing the wavelength of the incident light and recording the optical output power P_{out} versus the optical input power P_{in}. This is illustrated in Fig. 8, where P_{out} is plotted versus P_{in} for a set of wavelengths $\lambda_1-\lambda_3$ around the 1568 nm resonance, as indicated in Fig. 7(b). It is clear that a large variety in nonlinear transmission curves can be obtained by tuning the wavelength of the injected light. In Fig. 8(a), a limiting optical function is implemented when $\lambda=\lambda_1=1567.57$ nm, where the optical output power is limited to about 75 μW. In Fig. 8(b), high optical input powers are suppressed at the output when $\lambda=\lambda_2=1567.74$ nm, while in Fig. 8(c) low optical input powers are suppressed for $\lambda=\lambda_3=1567.97$ nm. These basic nonlinear responses can be used as building blocks for more complex digital photonic components, where the nonlinear transmission function of each individual ring can be tweaked by changing the input wavelength or by modifying the resonator dimensions.

VI. ALL-OPTICAL CONTROL OF OPTICAL DATA SIGNALS IN A III–V/SOI CAVITY

In Sec. V the resonance blueshift due to the creation of free carriers in the III–V overlay was discussed. Besides creating a strong nonlinear response, this effect can also be exploited to create an all-optically controlled modulator, as will be demonstrated below. By injecting a pump signal at a resonance wavelength of the III–V/SOI cavity, a fraction of the injected optical power (given by the extinction ratio of the particular resonance) will be dissipated in the III–V/SOI racetrack cavity. Part of this optical power will be absorbed in the InGaAsP active layer, thereby creating free carriers. This free carrier generation blueshifts all the resonances, thereby changing the transmission properties of the III–V/SOI racetrack resonator. As this blueshift affects all the resonances, the pump signal changes the transmission of a probe signal centered around another resonance of the racetrack resonator. The resonance blueshift of the probe signal transmission spectrum is illustrated in Figs. 9(a) and 9(b), where the transmission spectrum of the resonator is plotted around the 1548 nm resonance [case (a)] and 1568 nm resonance [case (b)] as a function of the pump signal power in the SOI waveguide, which is at a pump wavelength located at the

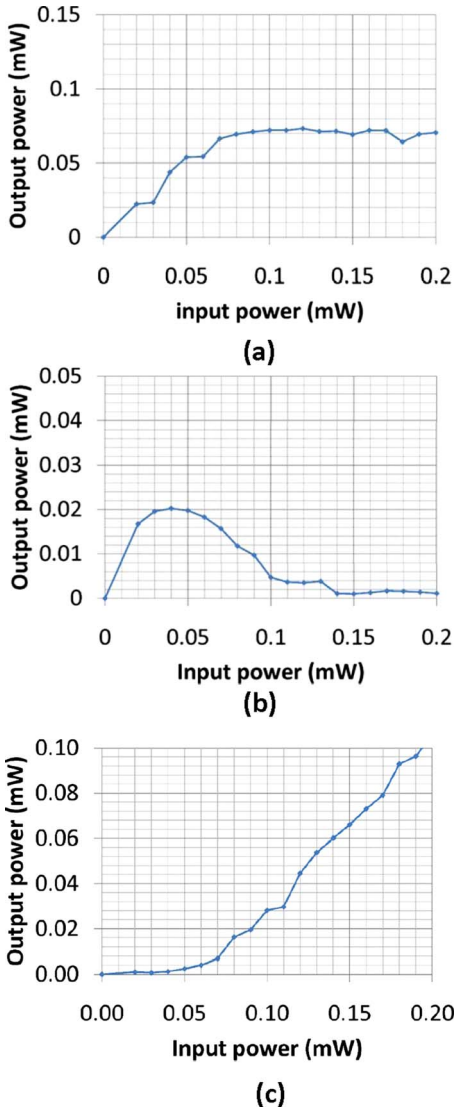

FIG. 8. (Color online) Nonlinear transmission characteristics in a III–V/SOI racetrack resonator for various optical input wavelengths: (a) optical limiter function, (b) suppression of high optical input power levels, and (c) suppression of low optical input power levels.

resonance around 1529 and 1548 nm, respectively. The 6.5 and 8 dB modulations of the probe signal can be obtained in the respective cases, with less than 500 μW of pump power. This is in sharp contrast with relatively high power levels that are required to achieve an all-optical modulation (wavelength conversion) in an all-silicon resonator, which relies on the relatively weak two-photon absorption to create free carriers and the free carrier plasma dispersion effect in silicon.[13] While thermal effects limit the amount of blueshift that can be obtained in continuous wave operation to about 0.3 nm, this is sufficient for all-optical modulation or switching as can be seen in Fig. 9. This is in contrast with all-silicon resonator devices, which suffer much more from these thermal effects, as discussed in Ref. 14, typically limiting the operation to a pulsed operation mode.

As this blueshift is due to carrier generation, the speed of this modulation is determined by the free carrier lifetime, which is about 500 ps. Higher operation speed can be obtained by applying a lateral electric field to sweep the carriers out of the active region,[14] thereby reducing the effective carrier lifetime.

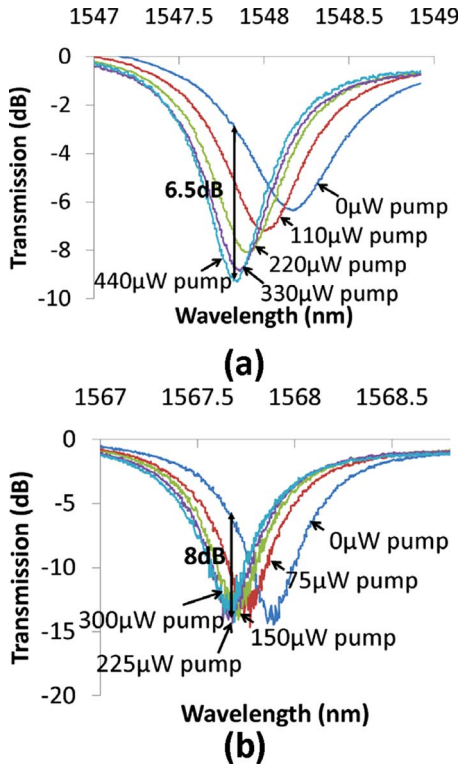

FIG. 9. (Color online) Resonator transmission spectrum as a function of pump signal power in the SOI waveguide: (a) resonance around 1548 nm, with a pump wavelength at the 1529 nm resonance, and (b) resonance around 1568 nm, with a pump wavelength at the 1548 nm resonance.

VII. CONCLUSIONS

In this paper, the use of hybrid III–V/SOI cavities as ultracompact light source and nonlinear optical element is presented. While light emission is only obtained using optical pumping, a whole set of applications could benefit from this type of device, i.e., in the research field of integrated optical sensing. In order to achieve lasing, the III–V/SOI cavity design needs to be further optimized. Besides the demonstrated all-optical modulation, a broad range of nonlinear optical functions, including optical logic, can be envisioned. The nonlinearity can even be further enhanced by replacing the quantum well layer structure with a quantum dot III–V active layer.

ACKNOWLEDGMENTS

This work was carried out in the framework of the Dutch Memphis SmartMix project and the COST MP0702 project. G. Roelkens acknowledges the Fund for Scientific Research Vlaanderen (FWO) for a postdoctoral grant. The authors would like to acknowledge Iwan Moreels, Bram De Geyter, and Professor Zeger Hens for the fruitful discussions.

[1]W. Bogaerts, R. Baets, P. Dumon, V. Wiaux, S. Beckx, D. Taillaert, B. Luyssaert, J. Van Campenhout, P. Bienstman, and D. Van Thourhout, J. Lightwave Technol. **23**, 401 (2005).
[2]K. Sasaki, F. Ohno, A. Motegi, and T. Baba, Electron. Lett. **41**, 801

(2005).
[3]P. Dumon, W. Bogaerts, V. Wiaux, J. Wouters, S. Beckx, J. Van Campenhout, D. Taillaert, B. Luyssaert, P. Bienstman, D. Van Thourhout, and R. Baets, IEEE Photonics Technol. Lett. **16**, 1328 (2004).
[4]Q. Xu, S. Manipatruni, B. Schmidt, J. Shakya, and M. Lipson, Opt. Express **15**, 430 (2007).
[5]J. Brouckaert, G. Roelkens, D. Van Thourhout, and R. Baets, IEEE Photonics Technol. Lett. **19**, 1484 (2007).
[6]L. Vivien, M. Rouvière, J.-M. Fédéli, D. Marris-Morini, J. F. Damlencourt, J. Mangeney, P. Crozat, L. El Melhaoui, E. Cassan, X. Le Roux, D. Pascal, and S. Laval, Opt. Express **15**, 9843 (2007).
[7]G. Roelkens, D. Van Thourhout, R. Baets, R. Nötzel, and M. Smit, Opt. Express **14**, 8154 (2006).
[8]A. W. Fang, R. Jones, H. Park, O. Cohen, O. Raday, M. J. Paniccia, and J. E. Bowers, Opt. Express **15**, 2315 (2007).
[9]J. Van Campenhout, P. Rojo Romeo, P. Regreny, C. Seassal, D. Van Thourhout, S. Verstuyft, L. Di Cioccio, J.-M. Fedeli, C. Lagahe, and R. Baets, Opt. Express **15**, 6744 (2007).
[10]H. Park, Y.-H. Kuo, A. W. Fang, R. Jones, O. Cohen, M. J. Paniccia, and J. E. Bowers, Opt. Express **15**, 13539 (2007).
[11]G. Roelkens, J. Brouckaert, D. Van Thourhout, R. Baets, R. Nötzel, and M. Smit, J. Electrochem. Soc. **153**, G1015 (2006).
[12]G. Roelkens, D. Van Thourhout, and R. Baets, Opt. Express **14**, 11622 (2006).
[13]Q. Xu and M. Lipson, Opt. Lett. **31**, 341 (2006).
[14]S. Preble, Q. Xu, B. Schmidt, and M. Lipson, Opt. Lett. **30**, 2891 (2005).